



OPEN

Size-dependent ability of AtaA to immobilize cells in *Acinetobacter* sp. Tol 5

Shogo Yoshimoto¹, Sota Aoki¹, Masahito Ishikawa², Atsuo Suzuki¹ & Katsutoshi Hori¹

Microbial cells serve as efficient and environmentally friendly biocatalysts, but their stability and reusability in practical applications must often be improved through immobilization. *Acinetobacter* sp. Tol 5 shows high adhesiveness to materials due to its large cell surface protein AtaA, which consists of 3630 amino acids (aa). Previously, we developed a method for immobilizing bacteria using AtaA. Herein, we investigated the cell immobilization ability of in-frame deletion (IFD) mutants of AtaA with different sizes in Tol 5. Mini-AtaA, which consists of 775 aa and is functional in *Escherichia coli*, was produced and present on the cell surface; however, mini-AtaA showed no immobilization ability in Tol 5. A cell immobilization assay was performed with cells expressing 16 IFD mutants of AtaA with different sizes, revealing that a length of at least 1417 aa was required for the sufficient immobilization of Tol 5 cells; thus, the minimum length needed to achieve the adhesive function of AtaA varies among bacterial species. The constructed mutant library of AtaA ranging from 3630 to 775 aa will allow researchers to quickly and easily explore the optimal size of AtaA, even for bacteria newly introduced to AtaA.

Keywords Autotransporter, Adhesion, Immobilization, Bacteria, Cell surface

Microbial cells can function as whole-cell biocatalysts that are highly effective and selective under ordinary temperature and atmospheric pressure; thus, these cells are used to produce compounds in an environmentally friendly manner^{1–4}. Cell immobilization is an important strategy for the successful application of whole-cell biocatalysts because it simplifies the product separation steps, increases the cell concentration, confers tolerance to toxic substances, and permits the repetitive or continuous use of valuable and expensive biocatalysts^{5–7}. Various immobilization methods, such as physical adsorption, chemical crosslinking, gel entrapment, and biofilm immobilization, have been developed and improved^{8–10}; however, these conventional methods involve practical limitations, such as mass transfer in the inner part of a gel, cell leakage from the support matrix, and adverse effects on cell viability and catalytic activity^{7,10,11}.

The gram-negative bacterium *Acinetobacter* sp. Tol 5 exhibits high adhesiveness to various material surfaces, including hydrophobic plastics, hydrophilic glass and metals, through its fibrous cell surface protein AtaA; this process is independent of cell growth and the secretion of extracellular polymeric substances (EPS)¹². AtaA is a member of the trimeric autotransporter adhesin (TAA) family¹³, and polypeptide chains of AtaA consisting of 3630 amino acids (aa) form a large homotrimeric fibrous structure that is over 1 MDa in molecular weight and 260 nm in length. TAAs, including AtaA, are secreted to the outer membrane (OM) by the type Vc secretion system^{14,15}. The large AtaA protein is composed of a notably long passenger domain (PSD) that is presented on the cell surface and exhibit biological functions and a C-terminal transmembrane domain (TM) that is anchored to the OM. The PSD consists of the N-terminal Ylhead (Nhead), the N-terminal stalk (Nstalk), the C-terminal Ylhead (Chead), and a C-terminal stalk (Cstalk), which are composed of several types of repeated domains and coiled-coil connectors^{16,17}.

We previously developed a method for immobilizing bacterial cells using AtaA¹⁸. Bacterial cells transformed with the AtaA gene exhibit nonspecific high adhesiveness, and large amounts of growing, resting, or even lyophilized transformant cells can be quickly and firmly immobilized onto any material surface according to the application¹⁹. Cells immobilized directly on surfaces through AtaA show better tolerance¹⁸ and increased chemical reaction rates and can be repeatedly used in reactions without inactivation¹⁹. Furthermore, the cells can be detached in deionized water but can be re-immobilized in fresh buffer solution²⁰.

¹Department of Biomolecular Engineering, Graduate School of Engineering, Nagoya University, Nagoya, Aichi 464-8603, Japan. ²Department of Frontier Bioscience, Faculty of Bioscience, Nagahama Institute of Bio-Science and Technology, Nagahama, Shiga 526-0829, Japan. ✉email: khorii@chembio.nagoya-u.ac.jp

However, the heterologous expression of AtaA in bacteria other than *Acinetobacter* is not easy due to the large molecular size of AtaA, and the practical application of the immobilization method is limited. Recently, we reported that Nhead is responsible for the adhesion of AtaA and constructed a miniaturized AtaA (mini-AtaA) that lacks most of the stalk²¹. Mini-AtaA was properly expressed in *E. coli*, allowing the immobilization of *E. coli* cells onto polyurethane carriers. This finding expanded the potential application of the immobilization method using AtaA; however, it is unknown why AtaA originally possesses this long stalk. In this study, we investigated the immobilization ability of in-frame deletion (IFD) mutants of AtaA that lack different domains.

Results

Immobilization of Tol 5 Δ ataA cells expressing mini-AtaA

To investigate the contribution of the stalk region of AtaA to adhesion in Tol 5, mini-AtaA (Fig. 1A) was expressed in the *ataA* gene knockout mutant strain of Tol 5 (Tol 5 Δ ataA). First, the protein production level in whole-cell lysates of Tol 5 Δ ataA cells expressing mini-AtaA was analyzed by immunoblotting with anti-AtaA₅₉₋₃₂₅ antiserum (Fig. 1B). Tol 5 Δ ataA cells expressing the full-length of AtaA (FL-AtaA) exhibited a single band corresponding to the expected molecular weight of 353 kDa, after the removal of the N-terminal signal peptide, which has a molecular weight of 6 kDa and is cleaved during translocation. Similarly, a single clear band corresponding to a molecular weight of 70 kDa for mini-AtaA was detected in the Tol 5 Δ ataA expressing mini-AtaA, indicating that mini-AtaA was produced without undesired degradation. Next, the cell surface expression of the proteins was examined by flow cytometry using anti-AtaA₅₉₋₃₂₅ antiserum. Compared to Tol 5 Δ ataA cells, cells expressing FL-AtaA and mini-AtaA showed similarly high fluorescence intensities (Fig. 1C). These results indicate that the mini-AtaA protein was properly produced in the Tol 5 Δ ataA cells and was present on the cell surface.

To evaluate the adhesiveness of cells expressing mini-AtaA, we conducted an immobilization assay using a polyurethane foam support. As controls, Tol 5 Δ ataA cells and those expressing FL-AtaA were also examined. After the cells were shaken for 60 min in the presence of the polyurethane foam support, the suspension of cells expressing FL-AtaA became clear, showing that most cells had adhered to the support (Fig. 2A). In contrast, the suspension of cells expressing mini-AtaA remained turbid, similar to that of Tol 5 Δ ataA, indicating that the cells had not adhered to the support. Subsequently, the immobilization ratio was quantified by measuring

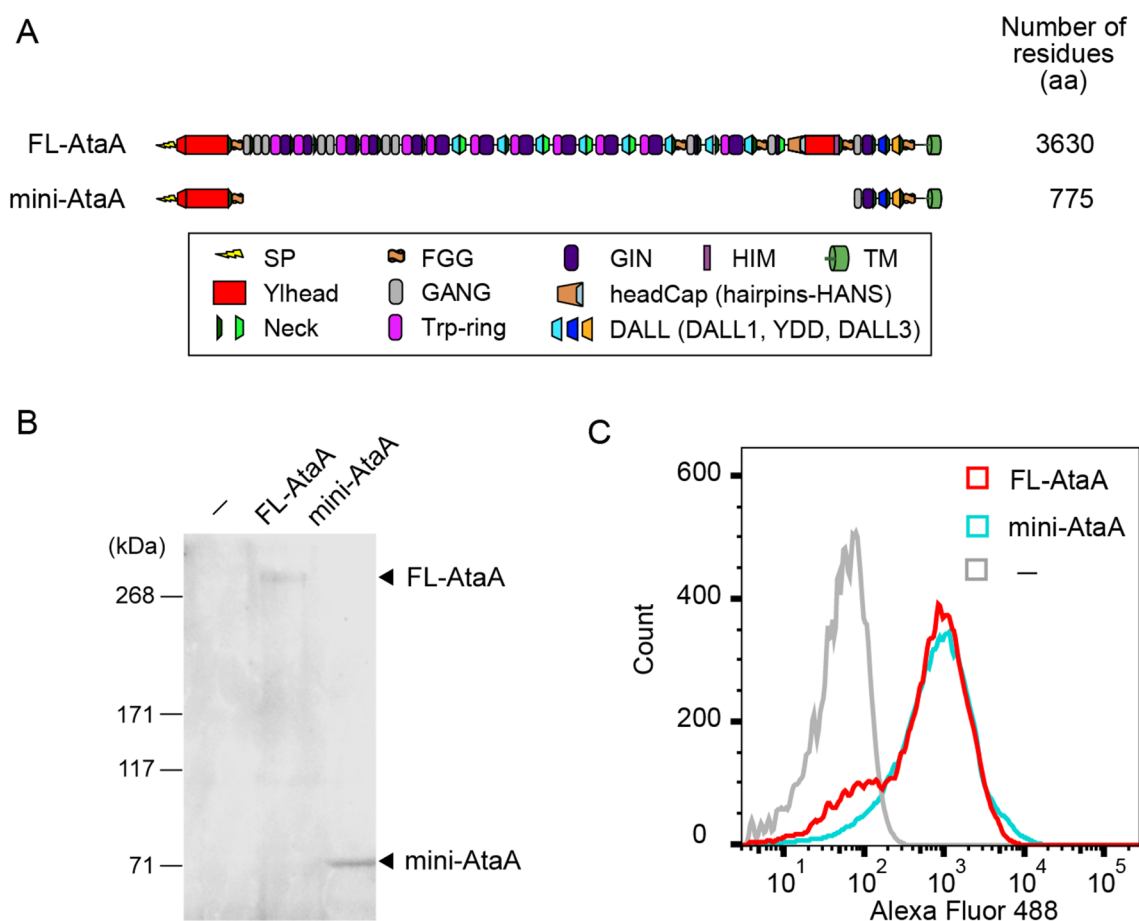


Fig. 1. Expression of mini-AtaA in Tol 5 Δ ataA. (A) Schematic representation of FL-AtaA and mini-AtaA. (B) Immunoblotting of whole-cell lysates of Tol 5 Δ ataA (-) and Tol 5 Δ ataA expressing FL-AtaA or mini-AtaA. The arrowheads indicate bands corresponding to FL-AtaA and mini-AtaA. (C) Flow cytometry of Tol 5 Δ ataA (-) and Tol 5 Δ ataA expressing FL-AtaA or mini-AtaA.

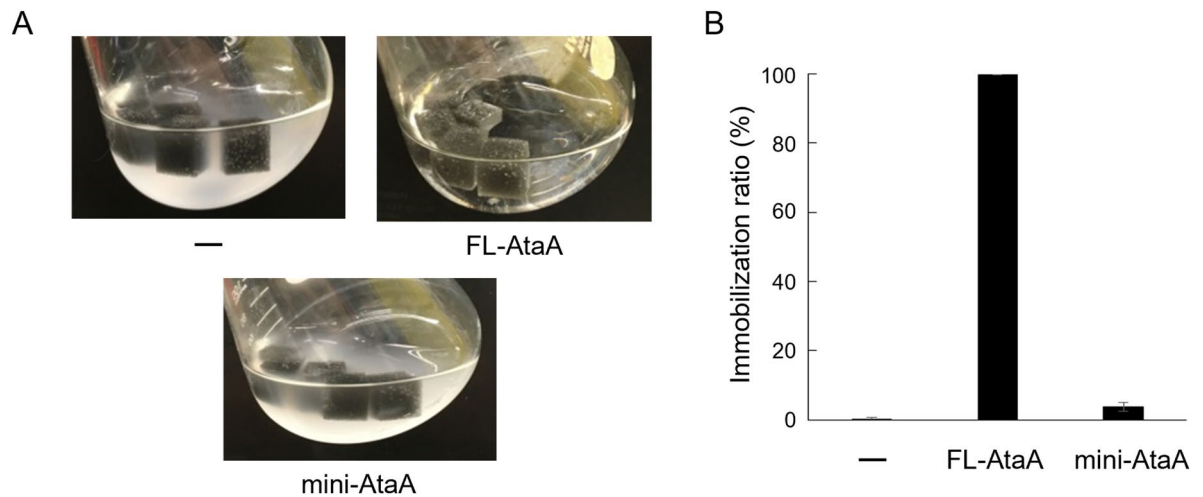


Fig. 2. Immobilization of Tol 5 Δ ataA (-) and Tol 5 Δ ataA expressing FL-AtaA or mini-AtaA on the polyurethane foam support. **(A)** Photographs of the bacterial cell suspension after shaking for 60 min with the support. **(B)** Immobilization ratio calculated from the decrease in the OD_{660} of the cell suspension after shaking. The data are presented as the means \pm SEMs ($n = 3$).

the change in optical density of the cell suspensions at 660 nm (OD_{660}) after shaking. The immobilization ratios were 99.7% for FL-AtaA, 0.19% for Tol 5 Δ ataA, and 3.7% for mini-AtaA (Fig. 2B). These results clearly indicate that mini-AtaA does not function in Tol 5 cells. Considering that more than 80% of the *E. coli* cells expressing mini-AtaA were immobilized in the same assay described previously²¹ and also reproduced here (Fig. S2), the minimum length of AtaA needed to exhibit high adhesiveness may differ among bacterial species.

Immobilization of Tol 5 Δ ataA cells expressing IFD mutants of AtaA with different sizes

We attempted to comprehensively evaluate the adhesive function of various AtaA mutants with amino acid residues between 3630 aa (FL-AtaA) and 775 aa (mini-AtaA). Our previous functional mapping studies showed that the deletion of Nhead significantly decreased adhesiveness, but partial deletions in the stalk region (Fig. 3A; IFD-1 to IFD-6) did not affect adhesiveness in Tol 5 Δ ataA²¹. Therefore, we designed 10 new IFD mutants that lacked more regions (Fig. 3A; IFD-7 to IFD-16). To design the new IFD mutants, we used the design method established in our previous study²²; this was performed to maintain the periodic sequence of coiled-coil regions before and after deletion, ensuring that the mutants did not suffer from structural distortions or steric clashes as shown in Fig. S2. In this way, we constructed a mutant library of AtaA, each variant retained the signal peptide, the adhesive domain Nhead, and the transmembrane domain, but varied in length.

An immobilization assay using a polyurethane foam support was conducted using Tol 5 Δ ataA cells that expressed each AtaA mutant from the library. The OD_{660} was measured periodically, and the immobilization ratio calculated from the decrease in the OD_{660} was plotted. For clarity, the results were shown in three divided panels (Fig. 3B–D). The immobilization ratio of cells expressing IFD-1 to IFD-12 reached nearly 100%, indicating that these mutants retained a high ability to immobilize cells, although IFD-12 showed a slower immobilization (Fig. 3B–D). On the other hand, the immobilization ratio of cells expressing IFD-13 to those expressing IFD-16 significantly decreased (Fig. 3D). The immobilization ratio obtained after the cells were shaken for 60 min was plotted on the graph, with the number of amino acid residues in the mutants on the x-axis and the immobilization ratio on the y-axis; the results showed that changes in the immobilization ratio were dependent on the number of amino acids in the mutants from IFD-12 to IFD-16 (Fig. 3E).

To examine whether the IFD mutants with reduced immobilization ability were properly produced in Tol 5 Δ ataA cells, immunoblotting was performed with whole-cell lysates of cells expressing each IFD using an antibody against AtaA_{3524–3630}. Clear bands corresponding to the theoretical molecular weight of the mutants were detected (Fig. 4A), indicating that protein production in the cells was normal. Next, to examine whether the mutants were present on the cell surface, flow cytometry with anti-AtaA_{59–325} antiserum was conducted. The fluorescence intensity of cells expressing IFD-12 to IFD-16 was comparable to or greater than that of cells expressing FL-AtaA (Fig. 4B). These results indicate that each IFD mutant was properly present on the cell surface. Therefore, even though the cell surface presentation of IFD-13 to IFD-16 was similar or higher than that of FL-AtaA, their cell immobilization ability was significantly lower than that of FL-AtaA. This finding implies that a decrease in the length of the stalk of AtaA negatively affects its immobilization in Tol 5.

Discussion

In this study, we found that mini-AtaA, which can perform cell immobilization in *E. coli*, did not function in Tol 5 Δ ataA cells. Furthermore, cell immobilization assay for the mutant library of different sizes of AtaA revealed that size-dependent adhesion of AtaA and a length of at least 1417 aa were necessary for sufficient adhesion in Tol 5 Δ ataA cells. This length was approximately twice as long as mini-AtaA, which consists of 775 aa and works in *E. coli*.

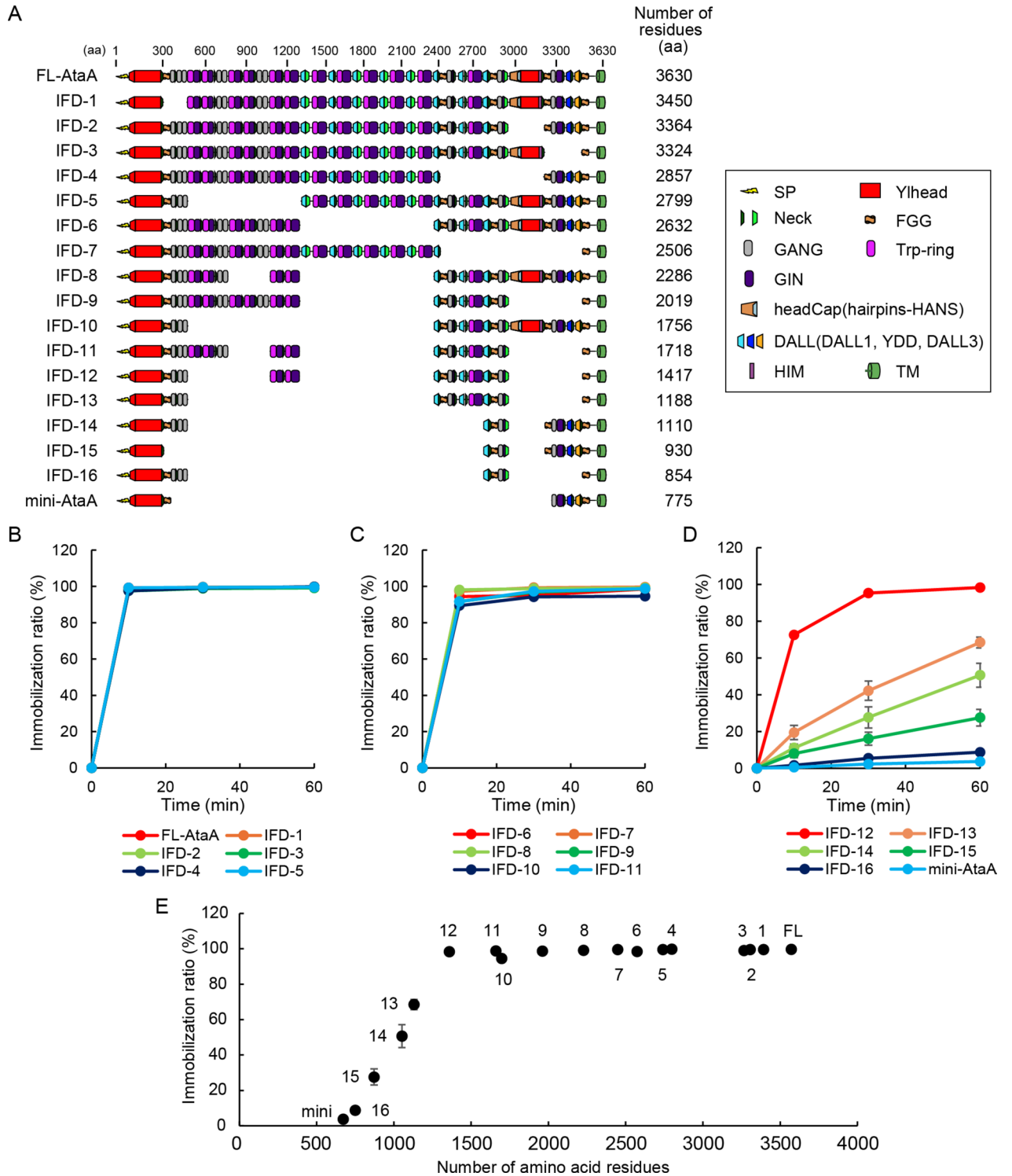


Fig. 3. Immobilization of Tol 5 *ΔataA* cells expressing mutant proteins of AtaA with different sizes. **(A)** Schematic representation of IFD mutant proteins of AtaA. **(B–D)** Immobilization ratio of Tol 5 *ΔataA* expressing **(B)** FL-AtaA and IFD-1 to IFD-5, **(C)** IFD-6 to IFD-11, **(D)** IFD-12 to IFD-16 and mini-AtaA, calculated from a decrease in the OD₆₆₀ of the cell suspension after shaking. **(E)** The immobilization ratio after shaking for 60 min was plotted with the number of amino acid residues of the mutants on the x-axis. The data are presented as the means ± SEMs (n = 3). Note that error bars are not visible in some of the plots because the data variation was minimal.

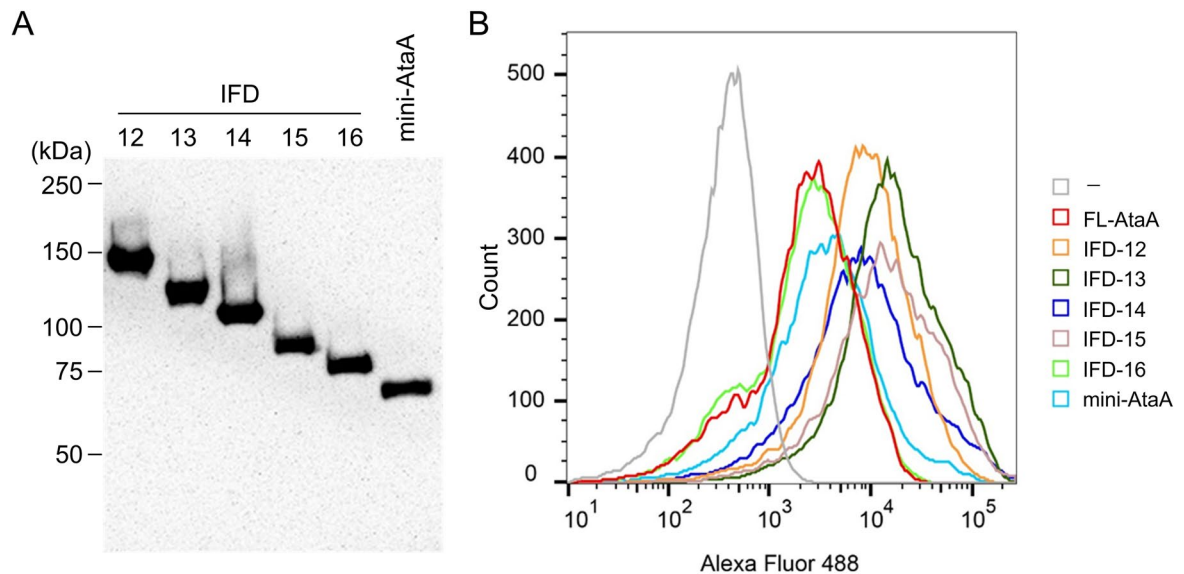


Fig. 4. Expression of IFD mutant proteins with reduced immobilization ability in Tol 5 Δ ataA. (A) Immunoblotting of the whole-cell lysates of Tol 5 Δ ataA expressing IFD-12 to IFD-16 and mini-AtaA. (B) Flow cytometry of Tol 5 Δ ataA (-) and Tol 5 Δ ataA expressing FL-AtaA, IFD-12 to IFD-16, and mini-AtaA.

It is generally believed that long fibrous proteins serve as spacers to present functional domains beyond the cell surface structures, such as other fiber proteins, lipopolysaccharides (LPS), and components of the cell wall^{23–25}. For Tol 5, a proteome analysis revealed that many types of fiber proteins were expressed, and transmission electron microscopy showed that at least some of these fiber proteins were present on the cell surface^{26,27}. These fiber proteins on Tol 5's cell surface may have obstructed the adhesion of the shorter AtaA mutants. Therefore, the very long stalk region of AtaA may also be important for presenting the adhesion domain Nhead, beyond these cell surface structures. In other TAAs, stalk domains have been reported to have various functions, such as adhesion to fibronectin, vitronectin, immunoglobulin G, and host cell receptors, as well as bending and serum resistance^{28–32}. Because AtaA stalk has diverse domains such as Neck, FGG, GANG, Trp-ring, DALL, GIN, and coiled coils, it is possible that some of them possess another unidentified function.

AtaA can be utilized to immobilize bacterial cells for efficient use in bioproduction processes¹⁸. However, the large size of AtaA significantly hinders heterologous protein production in host bacteria other than *Acinetobacter*. Previous studies improved the expression of AtaA in *E. coli* and achieved successful cell immobilization by reducing the size of AtaA from 3630 to 775 aa²¹. In contrast, this study revealed that a length of at least 1417 aa was necessary for sufficient adhesion of AtaA for Tol 5. This finding suggested that the minimum length needed for AtaA to exhibit its adhesive function varies among bacterial species. Given these insights, it is crucial to employ an AtaA mutant of an appropriate size for each bacterium used in bioprocesses. The mutant library of AtaA constructed in this study consists of 16 mutants with varying lengths ranging from 3450 to 775 aa (Fig. 3). Utilizing this library allows researchers to quickly and easily explore the optimal size of AtaA, even for bacteria newly introduced to AtaA. Therefore, this study will contribute to the development of bacterial immobilization technology using AtaA and the development of environmentally friendly production processes using immobilized bacteria as whole-cell catalysts.

Methods

Bacterial strains and culture conditions

The bacterial strains used in this study are listed in Supplementary Table S1. These bacterial strains were grown as described previously¹². *Acinetobacter* sp. Tol 5 and its mutant strains were grown at 28 °C, and *E. coli* strains were grown at 37 °C in lysogeny broth (LB) medium unless otherwise noted. The following antibiotics were used at the following concentrations when necessary: ampicillin (500 µg/mL) and gentamicin (10 µg/mL) for the Tol 5 mutant strains and ampicillin (100 µg/mL), gentamicin (10 µg/mL) and kanamycin (50 µg/mL) for the *E. coli* strains. For the expression of *ataA* and its mutants, an overnight culture of bacterial cells harboring the expression vector was inoculated into LB medium supplemented with ampicillin, gentamicin, and 0.5% (w/v) arabinose to induce the expression of genes under the control of the P_{BAD} promoter, and the medium was incubated for 7 h at 115 rpm.

Construction of plasmids

The plasmids and primers used in this study are listed in Supplementary Tables S2 and S3. The procedures for constructing IFD mutants in pDONR221 plasmids are described below.

To construct pIFD-7, a DNA fragment excised from pTAKN-2::Trp11_047&048²¹ with BglIII/BamHI was inserted into the BamHI site of pMD19::FragB²¹. A DNA fragment excised from the generated plasmid with BglIII/BamHI was inserted into the BamHI site of pMD19::FragA²¹, generating pMD19::FragAB_047&048. A

DNA fragment was amplified by inverse PCR (iPCR) from pDONR221::*ataA* using primers IFD7-f/IFD-7-r and self-ligated, generating pDONR221::IFD036b. A DNA fragment excised from pMD19::FragAB_047&048 with BglII/BsaI was inserted into the BamHI/BsaI site of pDONR221::IFD036b, generating pDONR221::IFD-7.

To construct pIFD-8, a DNA fragment excised from pTAKN-2::FragTrp5,6²¹ with BsaI/BamHI was inserted into the same site of pDONR221::FragA2-031²¹, generating pDONR221::FragA2-031_Trp5,6. A DNA fragment excised from pMD19::FragC²¹ with BglII/BamHI was inserted into the BamHI site of pDONR221::FragA2-031_Trp5,6, generating pDONR221::IFD-8.

To construct pIFD-9, a DNA fragment was amplified by iPCR from pTA2::AtaA2842-3630 using primers IFD9-f/IFD9-r and self-ligated, generating pTA2::dCheadCstalk. A DNA fragment excised from pTA2::dCheadCstalk with BglII/XbaI was inserted into the same site of pDONR221::IFD-6, generating pDONR221::IFD-9.

To construct pIFD-10, DNA fragments were amplified by PCR from pDONR221::IFD-5 using primers IFD10-f1/IFD10-r1 and IFD10-f2/IFD10-r2, excised with EcoRI/BamHI and BamHI/XbaI, respectively, and ligated into the EcoRI/XbaI site of pDONR221, generating pDONR221::IFD08c. A DNA fragment was amplified by PCR from pTA2::FragC using primers IFD10-f3/IFD10-r3 and sub-cloned into pTA2, generating pTA2::FragC_10. A DNA fragment excised from pTA2::FragC_10 with BsaI/BamHI was inserted into the same site of pDONR221::IFD08c, generating pDONR221::IFD-10.

To construct pIFD-11, a DNA fragment excised from pTA2::dCheadCstalk with BglII/XbaI was inserted into the same site of pDONR221::IFD-8, generating pDONR221::IFD-11.

To construct pIFD-12, a DNA fragment excised from pTAKN-2::FragTrp5,6 with BsaI/BamHI was inserted into the same site of pDONR221::IFD08c, generating pDONR221::IFD08c_Trp56. A DNA fragment excised from pMD19::FragC with BglII/BamHI was inserted into the BamHI site of pDONR221::IFD08c_Trp56, generating pDONR221::IFD-12c. A DNA fragment excised from pTA2::dCheadCstalk with BglII/XbaI was inserted into the same site of pDONR221::IFD-12c, generating pDONR221::IFD-12.

To construct pIFD-13, a DNA fragment excised from pTA2::dCheadCstalk with BglII/XbaI was inserted into the same site of pDONR221::IFD-10, generating pDONR221::IFD-13.

To construct pIFD-14, a DNA fragment was amplified by iPCR from pDONR221::IFD-10 using primers IFD14-f1/IFD14-r1 and self-ligated, generating pDONR221::IFD-10c. A DNA fragment was amplified by iPCR from pDONR221::IFD-10c using primers IFD14-f2/IFD14-r2 and self-ligated, generating pDONR221::IFD-14.

To construct pIFD-15, a DNA fragment was amplified by iPCR from pDONR221::IFD-14 using primers IFD14-f/IFD15-r and self-ligated, generating pDONR221::IFD-15.

To construct pIFD-16, a DNA fragment was amplified by iPCR from pDONR221::IFD-14 using primers IFD16-f/IFD16-r and self-ligated, generating pDONR221::IFD-16.

All of these *ataA* mutants in pDONR221 plasmids were excised with EcoRI/XbaI and inserted into the same site of pARP3, generating plasmids for expression. Transformation of the Tol 5 Δ *ataA* cells with these expression vectors was carried out by conjugal transfer from the *E. coli* S17-1 as previously described¹².

Protein detection

The expression and production of AtaA mutants were detected by SDS-PAGE followed by immunoblotting as described previously¹² with slight modifications. To confirm that AtaA and its mutants were produced, SDS sample buffer (5% (v/v) 2-mercaptoethanol, 2% (w/v) SDS, 0.02% (w/v) bromophenol blue, and 62.5 mM Tris-HCl, pH 6.8) supplemented with 8 M urea and anti-AtaA₅₉₋₃₂₅ rabbit antiserum²² was used. Flow cytometry was performed using anti-AtaA₅₉₋₃₂₅ rabbit antiserum and Alexa Fluor 488-conjugated anti-rabbit antibody (Cell Signaling Technology, MA) as described previously²².

Immobilization assay using polyurethane foam support

The immobilization of bacterial cells on polyurethane foam supports was performed as described previously²⁰, with slight modifications. The bacterial cells were suspended in 25 ml of BS-N buffer at an OD₆₆₀ of 1.0 in a 100-mL Erlenmeyer flask. Five pieces of polyurethane foam support with a specific surface area of 50 cm²/cm³ (CFH-40; Inoac Corporation, Nagoya, Japan) in the shape of a cube (1 cm³) were placed into the cell suspension and shaken at 115 rpm at 28 °C for 60 min. During shaking, the OD₆₆₀ of the cell suspension was measured periodically. The immobilization ratio of the cells was calculated using the following equation:

$$\text{Immobilization ratio(\%)} = 100 \times (\text{OD}_{600 \text{ initial}} - \text{OD}_{600 \text{ after shaking}}) / \text{OD}_{600 \text{ initial}} \quad (1)$$

Data availability

All data generated or analyzed during this study are included in this published article.

Received: 27 June 2024; Accepted: 31 August 2024

Published online: 09 September 2024

References

1. Taher, E. & Chandran, K. High-rate, high-yield production of methanol by ammonia-oxidizing bacteria. *Environ. Sci. Technol.* **47**, 3167–3173 (2013).
2. Fukuda, H., Hama, S., Tamalampudi, S. & Noda, H. Whole-cell biocatalysts for biodiesel fuel production. *Trends Biotechnol.* **26**, 668–673 (2008).
3. Pollard, D. J. & Woodley, J. M. Biocatalysis for pharmaceutical intermediates: the future is now. *Trends Biotechnol.* **25**, 66–73 (2007).
4. Schmid, A. *et al.* Industrial biocatalysis today and tomorrow. *Nature* **409**, 258–268 (2001).

5. Lotti, M., Pleiss, J., Valero, F. & Ferrer, P. Enzymatic production of biodiesel: Strategies to overcome methanol inactivation. *Biotechnol. J.* **13**, 700155 (2018).
6. Lee, S. Y. & Kim, H. U. Systems strategies for developing industrial microbial strains. *Nat. Biotechnol.* **33**, 1061–1072 (2015).
7. Junter, G. A. & Jouenne, T. Immobilized viable microbial cells: from the process to the proteome... or the cart before the horse. *Biotechnol. Adv.* **22**, 633–658 (2004).
8. Es, I., Vieira, J. D. G. & Amaral, A. C. Principles, techniques, and applications of biocatalyst immobilization for industrial application. *Appl. Microbiol. Biotechnol.* **99**, 2065–2082 (2015).
9. Halan, B., Buehler, K. & Schmid, A. Biofilms as living catalysts in continuous chemical syntheses. *Trends Biotechnol.* **30**, 453–465 (2012).
10. Cassidy, M. B., Lee, H. & Trevors, J. T. Environmental applications of immobilized microbial cells: A review. *J. Ind. Microbiol.* **16**, 79–101 (1996).
11. Carballeira, J. D. *et al.* Microbial cells as catalysts for stereoselective red-ox reactions. *Biotechnol. Adv.* **27**, 686–714 (2009).
12. Ishikawa, M., Nakatani, H. & Hori, K. AtaA, a new member of the trimeric autotransporter adhesins from *Acinetobacter* sp. Tol 5 mediating high adhesiveness to various abiotic surfaces. *PLoS One* **7**, e48830 (2012).
13. Linke, D., Riess, T., Autenrieth, I. B., Lupas, A. & Kempf, V. A. J. Trimeric autotransporter adhesins: Variable structure, common function. *Trends Microbiol.* **14**, 264–270 (2006).
14. Fan, E. G., Chauhan, N., Udata, D. B. R. K. G., Leo, J. C. & Linke, D. Type V secretion systems in bacteria. *Microbiol. Spectr.* <https://doi.org/10.1128/microbiolspec.VMBF-0009-2015> (2016).
15. Meuskens, I., Saragliadis, A., Leo, J. C. & Linke, D. Type V secretion systems: An overview of passenger domain functions. *Front. Microbiol.* **10**, 1163 (2019).
16. Koiwai, K., Hartmann, M. D., Linke, D., Lupas, A. N. & Hori, K. Structural basis for toughness and flexibility in the C-terminal passenger domain of an *Acinetobacter* trimeric autotransporter adhesin. *J. Biol. Chem.* **291**, 3705–3724 (2016).
17. Bassler, J., Alvarez, B. H., Hartmann, M. D. & Lupas, A. N. A domain dictionary of trimeric autotransporter adhesins. *Int. J. Med. Microbiol.* **305**, 265–275 (2015).
18. Ishikawa, M., Shigemori, K. & Hori, K. Application of the adhesive bacterionanofiber AtaA to a novel microbial immobilization method for the production of indigo as a model chemical. *Biotechnol. Bioeng.* **111**, 16–24 (2014).
19. Hori, K., Ohara, Y., Ishikawa, M. & Nakatani, H. Effectiveness of direct immobilization of bacterial cells onto material surfaces using the bacterionanofiber protein AtaA. *Appl. Microbiol. Biotechnol.* **99**, 5025–5032 (2015).
20. Yoshimoto, S., Ohara, Y., Nakatani, H. & Hori, K. Reversible bacterial immobilization based on the salt-dependent adhesion of the bacterionanofiber protein AtaA. *Microb. Cell Fact.* **16**, 123 (2017).
21. Yoshimoto, S. *et al.* Identification of the adhesive domain of AtaA from *Acinetobacter* sp. Tol 5 and its application in immobilizing *Escherichia coli*. *Front. Bioeng. Biotechnol.* **10**, 19557 (2023).
22. Aoki, S. *et al.* Native display of a huge homotrimeric protein fiber on the cell surface after precise domain deletion. *J. Biosci. Bioeng.* **129**, 412–417 (2020).
23. Hasman, H., Chakraborty, T. & Klemm, P. Antigen-43-mediated autoaggregation of *Escherichia coli* is blocked by fimbriation. *J. Bacteriol.* **181**, 4834–4841 (1999).
24. Mikula, K. M., Kolodziejczyk, R. & Goldman, A. *Yersinia* infection infection tools-characterization of structure and function of adhesins. *Front. Cell. Infect. Microbiol.* **2**, 169 (2013).
25. Formosa-Dague, C., Speziale, P., Foster, T. J., Geoghegan, J. A. & Dufrène, Y. F. Zinc-dependent mechanical properties of *Staphylococcus aureus* biofilm-forming surface protein SasG. *Proc. Natl. Acad. Sci. U.S.A.* **113**, 410–415 (2016).
26. Hori, K. *et al.* Production of peritrichate bacterionanofibers and their proteinaceous components by *Acinetobacter* sp. Tol 5 cells affected by growth substrates. *J. Biosci. Bioeng.* **111**, 31–36 (2011).
27. Inoue, S., Yoshimoto, S. & Hori, K. A new target of multiple lysine methylation in bacteria. *bioRxiv* <https://doi.org/10.1101/2024.1105.1115.594293> (2024).
28. Laarmann, S., Cutter, D., Juehne, T., Barenkamp, S. J. & St Geme, J. W. The *Haemophilus influenzae* Hia autotransporter harbours two adhesive pockets that reside in the passenger domain and recognize the same host cell receptor. *Mol. Microbiol.* **46**, 731–743 (2002).
29. Leo, J. C. *et al.* The structure of *E. coli* IgG-binding protein D suggests a general model for bending and binding in trimeric autotransporter adhesins. *Structure* **19**, 1021–1030 (2011).
30. Azari, F., Radermacher, M., Mintz, K. P. & Ruiz, T. Correlation of the amino-acid sequence and the 3D structure of the functional domain of EmaA from *Aggregatibacter actinomycetemcomitans*. *J. Struct. Biol.* **177**, 439–446 (2012).
31. Connors, R. *et al.* The *Moraxella* adhesin UspA1 binds to its human CEACAM1 receptor by a deformable trimeric coiled-coil. *EMBO J.* **27**, 1779–1789 (2008).
32. Leduc, I., Olsen, B. & Elkins, C. Localization of the domains of the *Haemophilus ducreyi* trimeric autotransporter DsrA involved in serum resistance and binding to the extracellular matrix proteins fibronectin and vitronectin. *Infect. Immun.* **77**, 657–666 (2009).

Acknowledgements

We thank Andrei N. Lupas and Dirk Linke for their kind discussions. We also thank Haruka Hirano and Eriko Kawamoto for their technical assistance. This work was supported by the Japan Society for the Promotion of Science (JSPS) KAKENHI (Grant Numbers JP24H00043, JP20H00319, and JP20K15098) and GteX Program Japan Grant number JPMJGX23B4.

Author contributions

S.Y. and K.H. conceptualized the study. S.Y. and S.A. performed the experiments. M.I. participated in the preliminary experiments. S.Y., S.A., M.I., A.S., and K.H. designed the mutant genes. S.Y. and K.H. prepared the manuscript. All authors approved the manuscript.

Competing interests

The authors declare no competing interests.

Additional information

Supplementary Information The online version contains supplementary material available at <https://doi.org/10.1038/s41598-024-71920-3>.

Correspondence and requests for materials should be addressed to K.H.

Reprints and permissions information is available at www.nature.com/reprints.

Publisher's note Springer Nature remains neutral with regard to jurisdictional claims in published maps and institutional affiliations.

Open Access This article is licensed under a Creative Commons Attribution-NonCommercial-NoDerivatives 4.0 International License, which permits any non-commercial use, sharing, distribution and reproduction in any medium or format, as long as you give appropriate credit to the original author(s) and the source, provide a link to the Creative Commons licence, and indicate if you modified the licensed material. You do not have permission under this licence to share adapted material derived from this article or parts of it. The images or other third party material in this article are included in the article's Creative Commons licence, unless indicated otherwise in a credit line to the material. If material is not included in the article's Creative Commons licence and your intended use is not permitted by statutory regulation or exceeds the permitted use, you will need to obtain permission directly from the copyright holder. To view a copy of this licence, visit <http://creativecommons.org/licenses/by-nc-nd/4.0/>.

© The Author(s) 2024